SOC Estimation of Lithium-Ion Batteries With AEKF and Wavelet Transform Matrix

Zhi-Liang Zhang, *Senior Member, IEEE*, Xiang Cheng, Zhou-Yu Lu, and Dong-Jie Gu

***Abstract*—Due to harsh electromagnetic environment in electric vehicle (EV), the measured current and voltage signals can be seriously polluted, which results in an estimation error of state of charge (SOC). The proposed denoising approach based on wavelet transform matrix (WTM) can analyze and denoise the nonstationary current and voltage signals effectively. This approach reduces the computation burden and is convenient to be programed in microcontroller unit, which is suitable for EV real-time application. The steps of the approach are as follows: 1) decomposition of the current and voltage signals based on WTM; 2) denoising of the wavelet coefficients under the thresholding rule; and 3) reconstruction of the denoised current and voltage signals based on inverse WTM. A battery-management system prototype was built to verify the approach on a Li(NiCoMn)O_2 battery module with nominal capacity of 200 Ah and rated voltage of 3.6 V. SOC estimation error with the proposed denoising approach is limited within 1%. Compared to the maximum error of 2.5% using an adaptive extended Kalman filter without denoising, an estimation error reduction of 1.5% is achieved.**

***Index Terms*—Signal denoising, state of charge (SOC), wavelet transform matrix (WTM).**

I. Introduction

TO GUARANTEE overall system performance, battery-management system (BMS) plays an important role in electric vehicle (EV). It monitors complete information of batteries to ensure safety and reliability, including the current and voltage. To prevent overcharging and overdischarging, thereby extending battery lifetime and preventing potential damage, these signals are normally used to estimate state of charge (SOC) and control battery balancing [1].

Due to electromagnetic interference from the high-power motor controller, motor, etc., the measured current and voltage signals are polluted by the stochastic and nonstationary noise, which imposes great challenge to SOC estimation accuracy. Meanwhile, the measured signals change drastically and randomly so that an effective manner that can analyze nonstationary signal and extract true signal from noisy signal is needed. Considering the inaccuracy of SOC estimation caused by the noisy voltage signal, the denoising approach based on wavelet basis of "dB3" was proposed [2], [3]. The aforementioned approach can denoise the noisy voltage signal effectively and increase SOC estimation accuracy. However, the noise contained in the current signal is ignored. At the same time, the program based on "dB3" basis involves convolution calculation and large amounts of cyclic functions. It is not convenient to be encoded in microcontroller unit (MCU) and is difficult to meet fast data processing requirement in real-time EV application.

An improved SOC estimation approach with adaptive extended Kalman filter (AEKF) and wavelet transform matrix (WTM) is proposed. The denoising approach based on WTM can analyze and denoise both of the noisy current and voltage signals. WTM is a sparse matrix and the denoising approach can be achieved by simple matrix multiplication. It contains no complex functions or large amounts of cyclic functions. Therefore, it reduces the computation complexity and is suitable for EV real-time application. AEKF that can adjust noise covariance is applied in this paper to realize precise SOC estimation [4], [5]. This approach has been validated on a Li(NiCoMn)O_2 battery module with the nominal capacity of 200 Ah and rated voltage of 3.6 V. The experimental results demonstrate that with the proposed denoising method, the maximum SOC estimation error is within 1%. Compared to the maximum error of 2.5% using AEKF without denoising, an estimation error reduction of 1.5% is achieved.

Section II gives the fundamentals and derivation of WTM. Section III presents the proposed SOC estimation approach with WTM and AEKF. Section IV demonstrates the experimental results and discussion. Section V provides a brief conclusion.

II. Fundamentals and Derivation of WTM

A. Fundamentals of Discrete Wavelet Transform (DWT)

Nowadays, DWT has been widely investigated as a popular mathematical tool that can decompose a time-domain signal into different frequency groups. It can provide the localization property in both the time and frequency domain. It is used as an effective manner to analyze the nonstationary signal compared to the traditional Fourier transform that can only give information in frequency domain. A variety of researches based on DWT have been implemented, including internal seal damage

Manuscript received July 31, 2016; revised October 19, 2016; accepted November 22, 2016. Date of publication December 6, 2016; date of current version May 9, 2017. This work was supported in part by the Natural Science Foundation of China under Grant 51577089, in part by the Lite-On Research Funding, in part by the Jiangsu Provincial Cooperative Innovation Fund-Prospective Joint Project (BY2015003-04), in part by the Fundamental Research Funds for Central Universities (NUAA) (NE2014101), and in part by the Foundation of Graduate Innovation Center in NUAA (KFJJ20160314). Recommended for publication by Associate Editor M. Ferdowsi.

The authors are with the Aero-Power Sci-Tech Center, Nanjing University of Aeronautics and Astronautics, Nanjing 211116, China (e-mail: zlzhang@nuaa.edu.cn; chengxiang@nuaa.edu.cn; luzy@nuaa.edu.cn; dongjiegu@nuaa.edu.cn).

Color versions of one or more of the figures in this paper are available online at http://ieeexplore.ieee.org.

Digital Object Identifier 10.1109/TPEL.2016.2636180

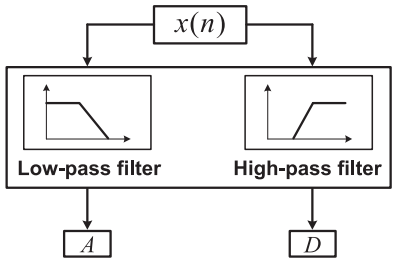

Fig. 1. Basic level of a wavelet transform filtering process.

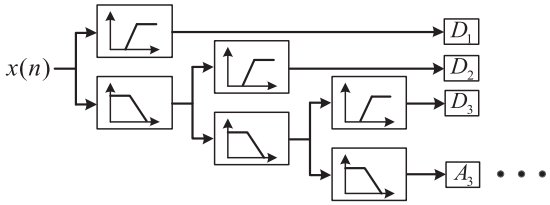

Fig. 2. Decomposition procedure of DWT-based MRA.

diagnosis [6], motor condition diagnosis [7], and denoising of signal and image [8]. DWT is defined as

$$\mathrm{DWT}(j,k)=\frac{1}{\sqrt{2^j}}\int_{\infty}^{\infty}x(t)\Psi^*\left(\frac{t-k2^j}{2^j}\right)dt \tag{1}$$

where *j* and *k* are scaling parameters of dilation and translation, respectively. $\Psi(t)$ is the mother wavelet function and the asterisk denotes the complex conjugate. It defines a dyadic-orthonormal wavelet transform and provides the basis for multiresolution analysis (MRA).

DWT is a MRA tool in which signal is divided into half-frequency bands at each level of decomposition, as shown in Fig. 1. DWT-based MRA can be implemented by using filter banks, as shown in Fig. 2. A_j is the approximation and D_j is the detail.

From Figs. 1 and 2, it can be known that any time signal $x(t)$ can be completely decomposed in terms of the approximations and details. At each level, the approximation A_j is divided into A_{j+1} with low frequency and D_{j+1} with high frequency. With successive approximations being decomposed in turn, one signal can be divided into many lower resolution components. For *n*-level decomposition, it can be described as

$$x(t)=A_n+D_1+D_2+D_3+\cdots+D_{n-1}+D_n. \tag{2}$$

The approximate component A_j is provided by the scaling function $\Phi_{j,k}(t)$ and the detailed component D_j is provided by the wavelet function $\Psi_{j,k}(t)$. These functions are described as

$$\Phi_{j,k}(t)=\ 2^{-\frac{j}{2}}\Phi(2^{-j}t-k) \tag{3}$$

$$\Psi_{j,k}(t)=\ 2^{-\frac{j}{2}}\Psi(2^{-j}t-k). \tag{4}$$

They are scaled and translated copies of $\Phi(t)$ and $\Psi(t)$ and associated with the low-pass filter coefficients $h(n)$ and high-pass filter coefficients $g(n)$, respectively

$$\Phi_{j,k}(t)=\ \sqrt{2}\sum_n h(n)\Phi(2t-n) \tag{5}$$

$$\Psi_{j,k}(t)=\ \sqrt{2}\sum_n g(n)\Phi(2t-n). \tag{6}$$

There are some important properties for filter coefficients

$$\sum_n h(n)=\ \sqrt{2},\ \sum_n g(n)=0 \tag{7}$$

$$\sum_n h(n)^2=\ 1,\ \sum_n g(n)^2=1 \tag{8}$$

$$h(L-1-n)=\ (-1)^n g(n) \tag{9}$$

where *L* is the filter length.

After the decomposition, the signal is divided into lower resolution components. The relationship of the approximation coefficients $a_{j,k}$ and detail coefficients $d_{j,k}$ between two adjacent levels at level *j* is described as

$$a_{j,k}=\ \sum_n h(n-2k)a_{j-1,n} \tag{10}$$

$$d_{j,k}=\ \sum_n g(n-2k)a_{j-1,n}. \tag{11}$$

Finally, *J*-level DWT representation of a signal $x(t)$ can be obtained as

$$x(t)=\ \sum_k a_{j,k}2^{-\frac{j}{2}}\Phi(2^{-j}t-k)+\sum_{j=1}^{J}\sum_k d_{j,k}2^{-\frac{j}{2}}\Psi(2^{-j}t-k) \tag{12}$$

where *J* is the number of decomposition level. The detail coefficients contain components generated by the noise. To denoise noisy signal, these coefficients should be adjusted. The denoised signal $x'(t)$ can be obtained with the reconstruction process.

B. Derivation of WTM

The Haar wavelet is the simplest orthonormal wavelet basis. It is memory efficient, computationally cheap, programming simple, and exactly reversible without the edge effects characteristic of other wavelets. Consequently, it is selected to construct WTM and implement wavelet analysis. The scaling function and wavelet function can be mathematically described as

$$\Phi(t)=\ \begin{cases}1,\ 0\le t<1\\ 0,\quad \text{other}\end{cases} \tag{13}$$

$$\Psi(t)=\ \begin{cases}1,\quad 0\le t<0.5\\ -1,\ 0.5\le t\le 1\\ 0,\quad \text{other}\end{cases}. \tag{14}$$

According to (5), (6) and the definition of Haar basis, $h(n)$ and $g(n)$ of second-order WTM can be obtained

$$h(n)=\ \begin{cases}\dfrac{1}{\sqrt{2}},\ n=0,1\\ 0,\quad \text{other}\end{cases} \tag{15}$$

$$g(n) = \begin{cases} \dfrac{1}{\sqrt{2}}, & n = 0 \\ -\dfrac{1}{\sqrt{2}}, & n = 1 \\ 0, & \text{other} \end{cases} \tag{16}$$

$h(n)$ and $g(n)$ meet the properties of low-pass and high-pass filter coefficients. After the decomposition, $a_{j,k}$ and $d_{j,k}$ can be derived from the relationship of these two coefficients at level j

$$a_{j,k} = \frac{1}{\sqrt{2}} a_{j-1,2k} + \frac{1}{\sqrt{2}} a_{j-1,2k+1} \tag{17}$$

$$d_{j,k} = \frac{1}{\sqrt{2}} a_{j-1,2k} - \frac{1}{\sqrt{2}} a_{j-1,2k+1}. \tag{18}$$

Therefore, for one-level decomposition, the second-order WTM can be obtained as

$$\mathrm{WTM}_{2\times 2} = \begin{bmatrix} \dfrac{1}{\sqrt{2}} & \dfrac{1}{\sqrt{2}} \\ \dfrac{1}{\sqrt{2}} & -\dfrac{1}{\sqrt{2}} \end{bmatrix}. \tag{19}$$

Based on (17), $a_{j-1,2k}$ and $a_{j-1,2k+1}$ can be derived as

$$a_{j-1,2k} = \frac{1}{\sqrt{2}} a_{j-2,4k} + \frac{1}{\sqrt{2}} a_{j-2,4k+1} \tag{20}$$

$$a_{j-1,2k+1} = \frac{1}{\sqrt{2}} a_{j-2,4k+2} + \frac{1}{\sqrt{2}} a_{j-2,4k+3}. \tag{21}$$

According to the above expressions, $a_{j,k}$, $d_{j,k}$, $d_{j-1,2k}$, and $d_{j-1,2k+1}$ can be obtained as

$$a_{j,k} = \frac{1}{2} a_{j-2,4k} + \frac{1}{2} a_{j-2,4k+1} + \frac{1}{2} a_{j-2,4k+2} + \frac{1}{2} a_{j-2,4k+3} \tag{22}$$

$$d_{j,k} = \frac{1}{2} a_{j-2,4k} + \frac{1}{2} a_{j-2,4k+1} - \frac{1}{2} a_{j-2,4k+2} - \frac{1}{2} a_{j-2,4k+3} \tag{23}$$

$$d_{j-1,2k} = \frac{1}{\sqrt{2}} a_{j-2,4k} - \frac{1}{\sqrt{2}} a_{j-2,4k+1} \tag{24}$$

$$d_{j-1,2k+1} = \frac{1}{\sqrt{2}} a_{j-2,4k+2} - \frac{1}{\sqrt{2}} a_{j-2,4k+3}. \tag{25}$$

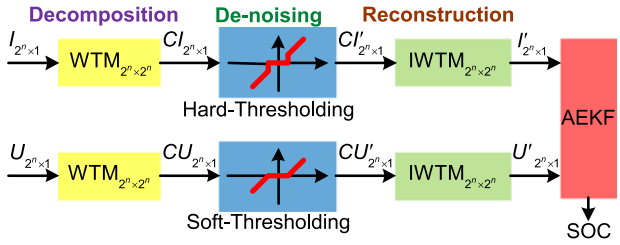

Fig. 3. Block diagram of the SOC estimation approach.

Therefore, for two-level decomposition, the fourth-order WTM can be obtained as

$$\mathrm{WTM}_{4\times 4} = \begin{bmatrix} \frac{1}{2} & \frac{1}{2} & \frac{1}{2} & \frac{1}{2} \\ \frac{1}{2} & \frac{1}{2} & -\frac{1}{2} & -\frac{1}{2} \\ \frac{1}{\sqrt{2}} & -\frac{1}{\sqrt{2}} & 0 & 0 \\ 0 & 0 & \frac{1}{\sqrt{2}} & -\frac{1}{\sqrt{2}} \end{bmatrix}. \tag{26}$$

With the recurrence to be carried out, for n-level decomposition, the 2^n-order WTM can be obtained as shown at the bottom of this page, where m is equal to $1/\sqrt{2}$. It can be observed that WTM based on Haar basis is a sparse matrix.

III. Proposed SOC Estimation Approach With WTM and AEKF

A. SOC Estimation With WTM and AEKF

The procedure of the SOC estimation approach is shown in Fig. 3. $I_{2^n\times1}$ and $U_{2^n\times1}$ are $2^n \times 1$ matrices of noisy current and voltage signals. $I'_{2^n\times1}$ and $U'_{2^n\times1}$ are $2^n\times1$ matrices of denoised current and voltage signals. $CI_{2^n\times1}$ and $CU_{2^n\times1}$ are $2^n \times 1$ matrices of wavelet coefficients after the decomposition of noisy signals. $CI'_{2^n\times1}$ and $CU'_{2^n\times1}$ are $2^n\times1$ matrices of denoised coefficients after the adjustment of wavelet coefficients.

From Fig. 3, it can be known that the decomposition can be accomplished with the 2^n-order WTM after sampling the noisy current and voltage signals. During the denoising process, the obtained wavelet coefficients are adjusted based on the thresholding rule. Afterward, these denoised wavelet coefficients are utilized to reconstruct the denoised current and voltage signals with the 2^n-order inverse WTM (IWTM). Finally, these denoised signals are applied in AEKF to estimate SOC.

$$\mathrm{WTM}_{2^n\times2^n} = \begin{bmatrix} m^n & m^n & \cdots & m^n & m^n & \cdots & m^n & m^n & \cdots & m^n & m^n & \cdots & m^n & m^n \\ m^n & m^n & \cdots & m^n & m^n & \cdots & m^n & -m^n & \cdots & -m^n & -m^n & \cdots & -m^n & -m^n \\ m^{n-1} & m^{n-1} & \cdots & m^{n-1} & -m^{n-1} & \cdots & -m^{n-1} & 0 & \cdots & 0 & 0 & \cdots & 0 & 0 \\ 0 & 0 & \cdots & 0 & 0 & \cdots & 0 & m^{n-1} & \cdots & m^{n-1} & -m^{n-1} & \cdots & -m^{n-1} & -m^{n-1} \\ \vdots & \vdots & \ddots & \vdots & \vdots & \ddots & \vdots & \vdots & \ddots & \vdots & \vdots & \ddots & \vdots & \vdots \\ m & -m & \cdots & 0 & 0 & \cdots & 0 & 0 & \cdots & 0 & 0 & \cdots & 0 & 0 \\ \vdots & \vdots & \ddots & \vdots & \vdots & \ddots & \vdots & \vdots & \ddots & \vdots & \vdots & \ddots & \vdots & \vdots \\ 0 & 0 & \cdots & 0 & 0 & \cdots & 0 & 0 & \cdots & 0 & 0 & \cdots & m & -m \end{bmatrix} \tag{27}$$

B. Detailed Procedure of the Proposed Denoising Approach

1) Decomposition of Noisy Current and Voltage Signals: The noisy current and voltage signals are measured continuously by BMS. After the measurement of 2^n current and voltage signals, the matrices of noisy signals can be obtained

$$I_{2^n\times 1} = [i_1, i_2, i_3, \cdots, i_{2^n-2}, i_{2^n-1}, i_{2^n}]^T \tag{28}$$

$$U_{2^n\times 1} = [u_1, u_2, u_3, \cdots, u_{2^n-2}, u_{2^n-1}, u_{2^n}]^T \tag{29}$$

where i_k and u_k are sampled current and voltage signals.

For *n*-level decomposition, the decomposition procedure can be described as

$$CI_{2^n\times 1} = \mathrm{WTM}_{2^n\times 2^n}\cdot I_{2^n\times 1} \tag{30}$$

$$CU_{2^n\times 1} = \mathrm{WTM}_{2^n\times 2^n}\cdot U_{2^n\times 1}. \tag{31}$$

After the decomposition, the wavelet coefficients matrices of noisy signals can be obtained

$$CI_{2^n\times 1} = [CIA_n, CID_n, CID_{n-1,1}, CID_{n-1,2}, CID_{n-2,1}, \cdots, CID_{1,2^{n-1}}]^T \tag{32}$$

$$CU_{2^n\times 1} = [CUA_n, CUD_n, CUD_{n-1,1}, CUD_{n-1,2}, CUD_{n-2,1}, \cdots, CUD_{1,2^{n-1}}]^T \tag{33}$$

where CIA_n and CUA_n are approximation coefficients of current and voltage signals at level *n*. $CID_{j,k}$ and $CUD_{j,k}$ are detail coefficients of current and voltage signals at level *j*. It can be observed that the quantity of detail coefficients at level *j* is twice as much as detail coefficients at level $j+1$.

2) Denoising Technique Based on the Thresholding Rule: After the decomposition, a series of wavelet coefficients are obtained. The energy of true signal is distributed over the coefficients with high magnitude. On the other hand, the energy of the noise is distributed over the coefficients with low magnitude. To eliminate the noise, these wavelet coefficients have to be adjusted under the thresholding rule [9].

The performance of the denoising technique depends on the threshold value δ_d. The *VisuShrink* which can perform visually calibrated adaptive smoothing on the noisy signal is used to determine the value [10]. It calculates the threshold value assuming that the noise has a random distribution. At level *j*, the threshold value $\delta_{d,j}$ can be calculated as

$$\delta_{d,j} = \sigma_j\sqrt{2\log N_d} \tag{34}$$

where N_d is the length of the coefficients vector. The unknown value σ_{j} can be calculated using median absolute deviation of the estimated noise from the wavelet coefficients at level *j*

$$\sigma_j = \frac{\mathrm{median}\left(\left\{CD_{j,k}|\, k=0,1,2,\cdots,2^j-1\right\}\right)}{0.6745} \tag{35}$$

where $CD_{j,k}$ is the detail coefficient at level *j*. Because the value σ_j is related to the detail coefficient $CD_{j,k}$, it can be known that a different threshold value is assigned to each level.

There are many options for the thresholding rule, however the hard thresholding and soft thresholding are representative [9]. The hard thresholding sets the detail coefficient to zero if the absolute value of the detail coefficient is lower than the threshold value, but keeps it unchanged if its absolute value is higher than the threshold value. It can be mathematically expressed as

$$CD'_{j,k} = \begin{cases} CD_{j,k} & |CD_{j,k}| \geq \delta_{d,j} \\ 0 & |CD_{j,k}| < \delta_{d,j} \end{cases}. \tag{36}$$

The soft thresholding sets the detail coefficient to zero if the absolute value of the detail coefficient is lower than the threshold value. If the absolute value is higher than the threshold value, it calculates the difference between the absolute value and threshold value. Afterward, it sets the detail coefficient to the difference according to the positive and negative sign of the detail coefficient. It can be mathematically expressed as

$$CD'_{j,k} = \begin{cases} \mathrm{sgn}(CD_{j,k})(|CD_{j,k}| - \delta_{d,j}) & |CD_{j,k}| \geq \delta_{d,j} \\ 0 & |CD_{j,k}| < \delta_{d,j} \end{cases}$$

$$\mathrm{sgn}(CD_{j,k}) = \begin{cases} +1, & CD_{j,k} \geq 0 \\ -1, & CD_{j,k} < 0 \end{cases} \tag{37}$$

The hard thresholding is chosen to denoise the current signal and the soft thresholding is chosen to denoise the voltage signal. After the adjustment of coefficients $CID_{j,k}$ and $CUD_{j,k}$, the denoised wavelet coefficients matrices of current and voltage signals can be obtained

$$CI'_{2^n\times 1} = [CIA_n, CID'_n, CID'_{n-1,1}, CID'_{n-1,2}, CID'_{n-2,1}, \cdots, CID'_{1,2^{n-1}}]^T \tag{38}$$

$$CU'_{2^n\times 1} = [CUA_n, CUD'_n, CUD'_{n-1,1}, CUD'_{n-1,2}, CUD'_{n-2,1}, \cdots, CUD'_{1,2^{n-1}}]^T \tag{39}$$

where $CID'_{j,k}$ and $CUD'_{j,k}$ are adjusted detail coefficients of current and voltage signals at level *j*.

3) Reconstruction of Current and Voltage Signals: The final step of the proposed denoising approach is the reconstruction of the current and voltage signals with the 2^n-order IWTM that can be derived from (27). The reconstruction procedure is

$$I'_{2^n\times 1} = \mathrm{IWTM}_{2^n\times 2^n}\cdot CI'_{2^n\times 1} \tag{40}$$

$$U'_{2^n\times 1} = \mathrm{IWTM}_{2^n\times 2^n}\cdot CU'_{2^n\times 1}. \tag{41}$$

After the reconstruction, the matrices of denoised current and voltage signals can be obtained

$$I'_{2^n\times 1} = [i'_1, i'_2, i'_3, \cdots, i'_{2^n-2}, i'_{2^n-1}, i'_{2^n}]^T \tag{42}$$

$$U'_{2^n\times 1} = [u'_1, u'_2, u'_3, \cdots, u'_{2^n-2}, u'_{2^n-1}, u'_{2^n}]^T \tag{43}$$

where i'_k and u'_k are the denoised current and voltage signals.

C. Battery Model and Flowchart of SOC Estimation

1) Battery Model: The equivalent circuit model is a popular model and its structure is shown in Fig. 4. u_{OCV} is OCV of battery and it is related to SOC. R_O is the internal resistance. R_{p1}, R_{p2}, C_{p1}, and C_{p2} are the polarization resistances and polarization capacitances. i_B is the battery current. u_B is the terminal voltage of the battery.

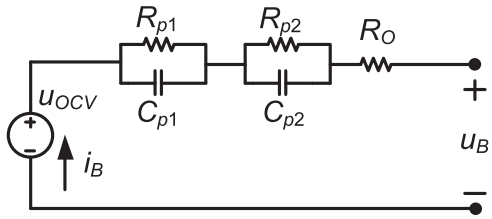

Fig. 4. Equivalent circuit model of the battery.

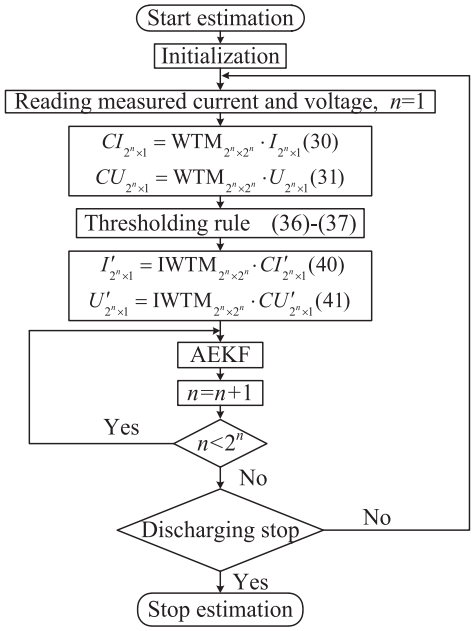

Fig. 5. Flowchart of the proposed approach.

2) Flowchart of an SOC Estimation Approach: Based on Fig. 4, the state transfer function and measurement function of AEKF can be constructed and battery SOC can be estimated [11]. To summarize the steps of the SOC estimation approach with WTM and AEKF, a detailed flowchart is shown in Fig. 5.

First, this approach reads 2^n sampled signals. In (30) and (31), WTM is used to decompose the noisy current and voltage signals. After the decomposition, the thresholding rule that can eliminate the wavelet coefficients generated by the noise is used in (36) and (37). Then, the denoised current and voltage signals can be reconstructed based on IWTM in (40) and (41). Finally, the denoised signals are applied in AEKF to estimate battery SOC. When 2^n denoised signals are all utilized, this approach reads next 2^n measured current and voltage signals and repeats this process.

D. Advantages of the Proposed Denoising Approach

In this paper, the proposed WTM can analyze and denoise nonstationary current and voltage signals. The procedure of decomposition and reconstruction can be completed by simple matrix multiplication. The 2^n-order WTM is a sparse matrix and the signal matrix and coefficient matrix are $2^n \times 1$ matrices. Therefore, this approach contains no complex functions or large amounts of cyclic functions, which reduces the computation complexity and is convenient to be programed in MCU. The updating time T of the signal matrix can be calculated as

$$T = 2^n \cdot \Delta t \tag{44}$$

where Δt is the sampling period of current and voltage signals. It can be known that the updating time T is proportional to the matrix order and signal sampling period. The signal sampling period is determined by the monitor chips. During the updating period of next signal matrix, the previous signal matrix can be denoised and the denoised signals are used to estimate SOC. Therefore, this approach can meet the real-time requirement in EV application. More detailed analysis about updating time is presented in Section IV.

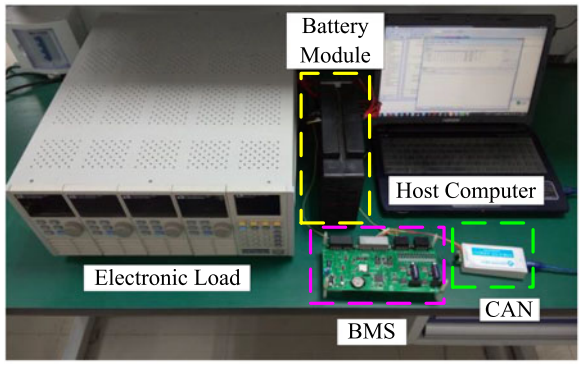

Fig. 6. Battery test bench.

IV. Experimental Results and Discussion

A BMS prototype was built and the test bench is shown in Fig. 6. This BMS is designed to monitor 24 series-connected battery modules with two LTC6803-4 battery stack monitor chips from the linear technology. The INA226 current shunt monitor chip from Texas Instruments is used to measure the battery current. A Li(NiCoMn)O_2 battery module with the nominal capacity of 200 Ah and rated voltage of 3.6 V from Do-Fluoride New Energy Technology, Co., Ltd., is used to validate the proposed approach. The voltage of the battery module ranges from 3.0 to 4.2 V. The electronic load is programed to simulate working current of EV. The host computer is used to transfer and record CAN message. The voltage sampling period with LTC6803-4 is 13 ms [12]. The current sampling period with INA226 is set to be 13 ms [13]. The denoising approach is implemented based on the 16-order WTM. Therefore, the updating period of signal matrix is 208 ms. During the updating period of next signal matrix, the previous signal matrix can be denoised and the denoised signals are used to estimate SOC. Therefore, we can obtain 16 estimated SOC values in about 208 ms and SOC update time can be limited to 13 ms.

A. Identification of Battery Module Parameters

To obtain the function between OCV and SOC, the battery module is charged and discharged at the rate of 8 A. During the

TABLE I
BATTERY MODULE PARAMETERS

Parameter	R_O (mΩ)	R_{p1} (mΩ)	C_{P1} (F)	R_{p2} (mΩ)	C_{P2} (F)
Value	0.3	0.13	440 000	0.13	80 000

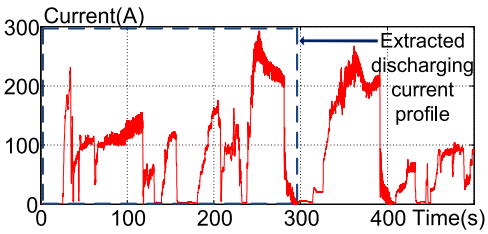

Fig. 7. Partial current profile of EV on driving condition.

test, the terminal voltage is monitored continuously and these data are transferred to the host computer. The battery OCV is simplified as the average value of charge and discharge voltage. Using MATLAB curve fitting tool, it is found that the function can be approximated perfectly by the eighth-order polynomial. The root-mean-squared error is limited to 0.0054. The eighth-order polynomial is given as

$$\begin{aligned} u_{\mathrm{OCV}} = & -465.5 \cdot \mathrm{SOC}^8 + 1998 \cdot \mathrm{SOC}^7 - 3538 \cdot \mathrm{SOC}^6 \\ & + 3335 \cdot \mathrm{SOC}^5 - 1805 \cdot \mathrm{SOC}^4 + 567.4 \cdot \mathrm{SOC}^3 \\ & - 100.5 \cdot \mathrm{SOC}^2 + 9.7 \cdot \mathrm{SOC} + 3.106. \end{aligned} \tag{45}$$

Other battery module parameters, such as internal resistance (R_O), polarization resistances $(R_{p1},\ R_{p2})$, and polarization capacitances (C_{p1}, C_{p2}) can be identified by the hybrid pulse power characteristic (HPPC) test [4]. In practice, the temperature and aging have effects on battery module parameters. Therefore, a battery model with varied parameters is normally necessary. In this paper, the temperature is remained at room temperature. At the same time, the parameters are identified before the verification experiment of SOC estimation. Therefore, the parameters can be considered as constants during an experiment. According to the data of voltage in HPPC test and voltage response expressions, the battery module parameters can be obtained with the assistance of MATLAB curve fitting tool. Table I shows the identification results.

B. Simulated Discharging Current and Noise

To simulate EV working current, the data of discharging current in real driving condition are needed. These data are recorded by the host computer via CAN transceiver when EV is on driving condition. The current profile is shown in Fig. 7, and the partial current profile is extracted to simulate the discharging current.

The approximate scaled-down discharging current profile which is extracted from Fig. 7 is presented in Fig. 8. The experimental discharging current profile is a repetition of the current profile. It is programed in the electronic load to simulate EV working current.

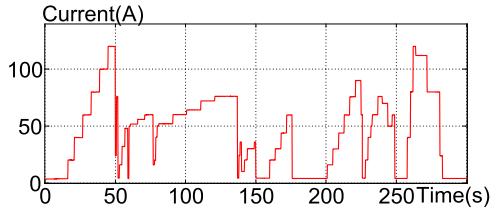

Fig. 8. Approximate scaled-down discharging current profile.

TABLE II
THRESHOLD VALUES OF SIGNALS AT EACH LEVEL

	Level 1	Level 2	Level 3	Level 4
Current	6.108	5.224	4.544	4.174
Voltage	0.00974	0.00561	0.00381	0.00201

To simulate the noise contained in the current and voltage signals, the noise signals are generated by the random function in MATLAB. The current noise sequence is subject to a normal distribution of $N(0,4)$. The voltage noise sequence is subject to a normal distribution of $N(0,0.000036)$. These noise signals are recorded by the host computer and sent to BMS via CAN transceiver. They are added to the measured current and voltage signals.

C. Denoising of Current and Voltage Signals

1) Denoising of Coefficients Based on Thresholding Rule: In this paper, the 16-order WTM is utilized to decompose the noisy current and voltage signals. Therefore, the four-level decomposition can be implemented for extracting information from noisy signals. After the decomposition, the wavelet coefficients at each level can be obtained. The detail coefficients generated by the noise are contained in these detail coefficients. The performance of the denoising technique depends on the threshold value. The threshold values of the current and voltage signals at each level are listed in Table II.

The hard thresholding and soft thresholding are selected to denoise the current and voltage signals, respectively. The detail coefficients CID_1–CID_4 of the current signals before and after denoising are shown in Figs. 9–12. The detail coefficients CUD_1–CUD_4 of the voltage signals before and after denoising are shown in Figs. 13–16. For a clear comparison, the zoomed figures of the detail coefficients are also presented. It can be observed that some of the denoised detail coefficients are smaller than the original detail coefficients. These detail coefficients have been adjusted based on the thresholding rule. Therefore, the small detail coefficients generated by the noise are eliminated effectively.

2) Reconstruction of Denoised Current and Voltage Signals: After the denoising of detail coefficients, the denoised coefficients of current and voltage signals can be obtained. The reconstruction of the denoised signals can be achieved based on the 16-order IWTM. The comparison of the current and voltage signals before and after denoising is shown in Figs. 17

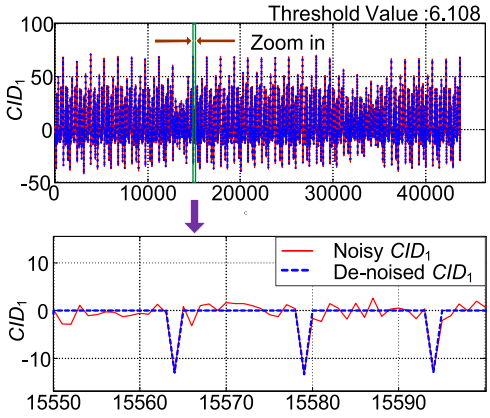

Fig. 9. Comparison of current detail coefficients CID_1.

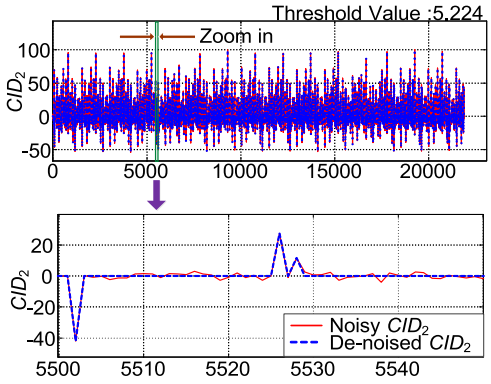

Fig. 10. Comparison of current detail coefficients CID_2.

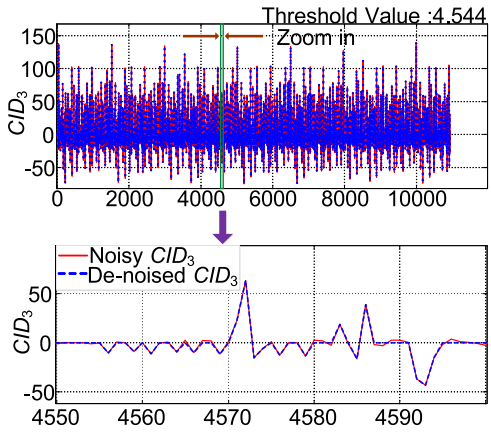

Fig. 11. Comparison of current detail coefficients CID_3.

and 18. For a clear comparison, the zoomed comparison figures are also presented. It can be observed that the original current and voltage signals are polluted by the random noise signals. After performing the denoising technique, the denoised signals are relatively smooth than the noisy signals. Therefore, the noise signals are reduced effectively.

The signal-to-noise ratio (SNR) value is used to evaluate the denoising capability. It is defined as the ratio of signal power to noise power. The higher SNR value means the better denoising performance. The comparison of SNR value before and after

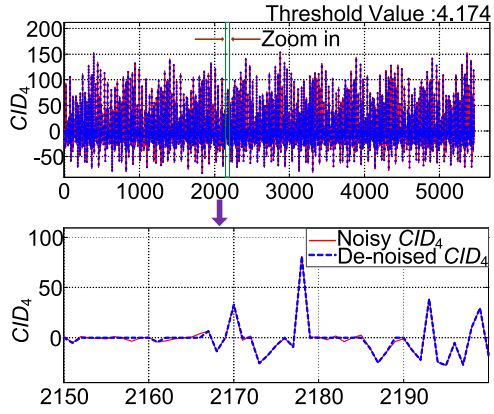

Fig. 12. Comparison of current detail coefficients CID_4.

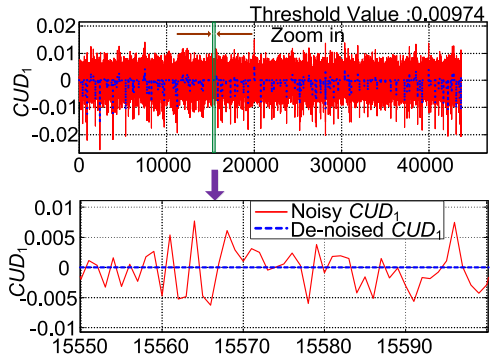

Fig. 13. Comparison of voltage detail coefficients CUD_1.

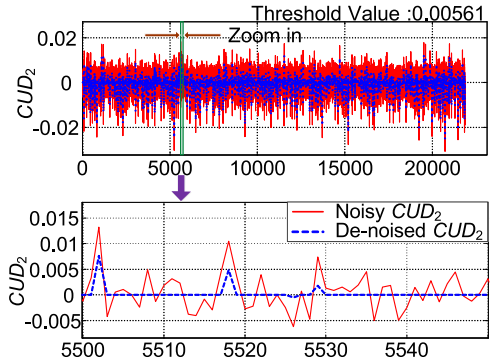

Fig. 14. Comparison of voltage detail coefficients CUD_2.

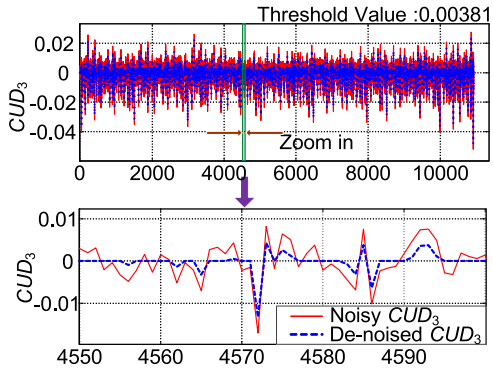

Fig. 15. Comparison of voltage detail coefficients CUD_3.

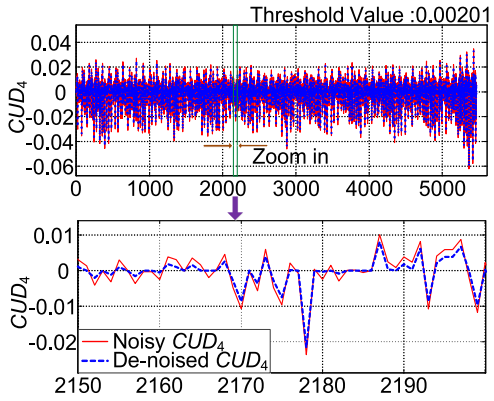

Fig. 16. Comparison of voltage detail coefficients CUD_4.

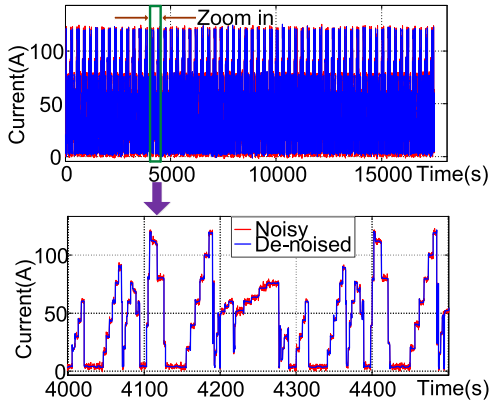

Fig. 17. Comparison between noisy and denoised current signal.

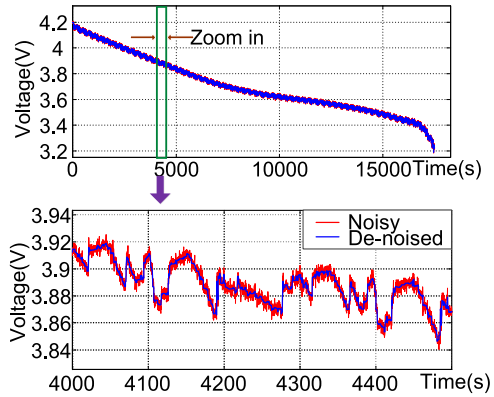

Fig. 18. Comparison between noisy and denoised voltage signal.

denoising is list in Table III. The increased SNR value of current and voltage signals is 5.0163 and 5.4162 dB, respectively. It can be known that after performing this denoising approach, the noise is eliminated effectively.

D. SOC Estimation With the Proposed Denoising Approach and AEKF

After the denoising of current and voltage signals, the denoised signals are applied to AEKF and the battery module

TABLE III
SNR VALUE OF SIGNALS BEFORE AND AFTER DENOISING

SNR	Before (dB)	After (dB)	Increased (dB)
Current	26.8103	31.8266	5.0163
Voltage	37.2559	42.6721	5.4162

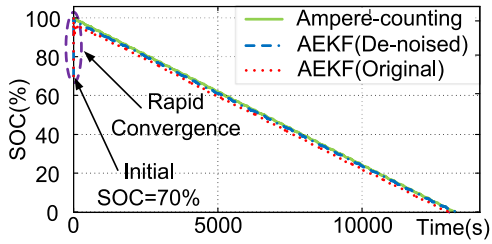

Fig. 19. SOC estimation comparison between AEKF (original) and AEKF (denoised).

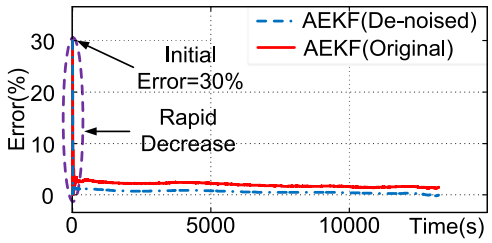

Fig. 20. SOC estimation error comparison between AEKF (original) and AEKF (denoised).

SOC can be estimated. The comparison between AEKF with and without denoising is shown in Fig. 19. The load current is programed in the electronic load, so the discharging current is known and precise enough. On the other hand, the capacity of the battery module and initial SOC can be measured precisely before the discharging experiment. Therefore, the ampere–hour counting can provide an accurate SOC and it is used as the benchmark. In order to validate the robustness of the SOC estimation approach, the initial SOC is set to 70%, while the true SOC is 100%. It is observed that the estimated SOC based on AEKF converges to the true SOC quickly.

The comparison of SOC estimation error between AEKF with and without denoising is shown in Fig. 20. It can be observed that the initial error is 30%. The error decreases rapidly in the following several seconds. It is also noted that SOC estimation error of AEKF with denoising is smaller than AEKF without denoising.

For a convenient comparison of SOC estimation error in steady state, the zoomed figure of SOC estimation error is shown in Fig. 21. Obviously, AEKF based on the denoised signal achieves better performance than AEKF without denoising. After the denoising of current and voltage signals, the maximum estimation error is within 1%. Compared to the maximum error of 2.5% for AEKF without denoising, an estimation error reduction of 1.5% can be obtained, which meets the accuracy requirement of SOC estimation.

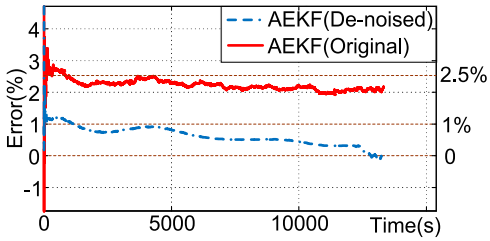

Fig. 21. Zoomed SOC estimation error comparison between AEKF (original) and AEKF(denoised).

V. Conculsion

The measured current and voltage signals are nonstationary and normally contain random noise which has great effects on SOC estimation. An improved SOC estimation approach with WTM and AEKF is proposed. The proposed denoising approach based on WTM can denoise the noisy current and voltage signals effectively. WTM is a sparse matrix and the denoising approach can be implemented by simple matrix multiplication. It contains no complex functions or large amounts of cyclic functions. Therefore, this approach reduces the computation burden and is convenient to be programed in MCU. Meanwhile, it reduces the computing time and is suitable for the real-time application in EV. This approach has been validated on a $Li(NiCoMn)O_2$ battery module with the nominal capacity of 200 Ah and rated voltage of 3.6 V. The experimental results demonstrate that with the proposed denoising method, the maximum SOC estimation error is within 1%. Compared to the maximum error of 2.5% using AEKF without denoising, an estimation error reduction of 1.5% is achieved.

Reference

[1] Z. Zhang, H. D. Gui, D. J. Gu, Y. Yang, and X. Ren, "A hierarchical active balancing architecture for lithium-ion batteries," *IEEE Trans. Power Electron.*, early press.

[2] J. Kim, C. Y. Chun, and B. H. Cho, "Implementation of EKF combined with discrete wavelet transform-based MRA for improved SOC estimation for a Li-ion cell," in *Proc. IEEE Appl. Power Electron. Conf.*, 2013, pp. 2720–2725.

[3] J. Kim and B. H. Cho, "Application of wavelet transform-based discharging charging voltage signals denoising for advanced data-driven SOC estimator," in *Proc. IEEE Appl. Power Electron. Conf.*, 2015, pp. 3013–3018.

[4] R. Xiong, H. W. He, F. C. Sun, and K. Zhao, "Evaluation on state of charge estimation of batteries with adaptive extended Kalman filter by experiment approach," *IEEE Trans. Veh. Technol.*, vol. 62, no. 1, pp. 108–117, Jan. 2013.

[5] H. W. He, R. Xiong, X. W. Zhang, F. C. Sun, and J. X. Fan, "State-of-charge estimation of the lithium-ion battery using an adaptive extended Kalman filter based on an improved thevenin model," *IEEE Trans. Veh. Technol.*, vol. 60, no. 4, pp. 1461–1469, May 2011.

[6] A. Y. Goharrizi and N. Sepehri, "A wavelet-based approach to internal seal damage diagnosis in hydraulic actuators," *IEEE Trans. Ind. Electron.*, vol. 57, no. 5, pp. 1755–1763, May 2010.

[7] M. R. Guasp, J. A. A. Daviu, M. P. Sanchen, R. P. Panadero, and J. P. Cruz, "A general approach for the transient detection of slip-dependent fault components based on thediscrete wavelet transform," *IEEE Trans. Ind. Electron.*, vol. 55, no. 12, pp. 4167–4180, Dec. 2008.

[8] L. Boubchir and B. Boashash, "Wavelet denoising based on the MAP estimation using the BKF with application to images and EEG signals," *IEEE Trans. Signal Process.*, vol. 61, no. 8, pp. 1880–1894, Apr. 2013.

[9] M. A. Farahani, M. T. V. Wylie, E. C. Guerra, and B. G. Colpitts, "Reduction in the number of averages required in BOTDA sensors using wavelet denoising techniques," *J. Lightw. Technol.*, vol. 30, no. 8, pp. 1134–1142, Apr. 2012.

[10] I. M. Johnstone and B. Silverman, "Wavelet threshold estimators for data with correlated noise," *J. Roy. Stat. Soc.*, vol. 59, no. 2, pp. 319–351, 1997.

[11] H. F. Dai, X. Z. Wei, Z. C. Sun, J. Y. Wang, and W. J. Gu, "Online cell SOC estimation of Li-ion battery packs using a dual time-scale Kalman filtering for EV applications," *J. Appl. Energy*, vol. 95, no. 2, pp. 227–237, 2012.

[12] LTC6803-4, Linear Technology. (2011). [Online]. Available: http://cds.linear.com/docs/en/datasheet/ 680324fa.pdf

[13] INA226, Texas Instruments. (2011). [Online]. Available: http://www.ti.com/lit/ds/symlink/ ina226.pdf

Zhi-Liang Zhang (S'03–M'09–SM'14) received the B.Sc. and M.Sc. degrees in electrical engineering from Nanjing University of Aeronautics and Astronautics (NUAA), Nanjing, China, in 2002 and 2005, respectively, and the Ph.D. degree from the Department of Electrical and Computer Engineering, Queen's University, Kingston, ON, Canada, in 2009.

In June 2009, he joined NUAA, where he is currently a Professor with the Aero-Power Sci-Tech Center. His research interests include high-frequency power converters and renewable energy power conversion system.

Dr. Zhang was the Winner of the "United Technologies Corporation Rong Hong Endowment" in 1999. He was the Secretary of the PELS Technical Committee on Power and Control Core Technologies from 2013 to 2016.

Xiang Cheng received the B.S. degree in electrical engineering from Nanjing University of Aeronautics and Astronautics, Nanjing, China, in 2015, where he is currently working toward the M.S. degree at the Aero-Power Sci-tech Center.

His research interests include renewable energy power converters and BMS.

Zhou-Yu Lu is currently working toward the B.S. degree in electrical engineering from Nanjing University of Aeronautics and Astronautics, Nanjing, China.

His research interests include high-frequency power converters.

Dong-Jie Gu received the B.S. degree in electrical engineering from Nanjing University of Aeronautics and Astronautics, Nanjing, China, in 2014, where he is currently working toward the M.S. degree at the Aero-Power Sci-Tech Center.

His research interests include renewable energy power converters.